Journal of Thermal Analysis and Calorimetry
https://doi.org/10.1007/s10973-025-14709-4

New calibration method for skin calorimeters without baseline correction for continuous heat flux measurement

Pedro Jesús Rodríguez de Rivera[1] · Miriam Rodríguez de Rivera[2] · Fabiola Socorro[1] · Manuel Rodríguez de Rivera[1]

Received: 19 July 2024 / Accepted: 11 August 2025

Abstract
In this study, we present a new calibration method for a skin calorimeter that allows continuous measurement on the skin without the need for baseline correction. This approach is essential for practical applications that require immediate and uninterrupted monitoring, such as in clinical and physiological studies. The skin calorimeter, designed to measure heat flux, heat capacity, and thermal resistance of a 2×2 cm^2 skin area, is calibrated using a small aluminum block with a built-in resistor and temperature sensor. Calibration was performed over a range of thermostat temperatures (26–32 ºC) and Peltier currents (25, 75, and 125 mA), resulting in an accurate model, with a root mean square error (RMSE) of less than 0.15 mW in power measurements. The calorimeter's performance was validated through experiments on human subjects, demonstrating accurate and reliable heat flux measurements without baseline correction. This method simplifies the measurement process and enhances the practical utility of skin calorimetry in various applications.

Keywords Conduction calorimetry · Direct calorimetry · Skin heat flux · Skin calorimeter · Skin thermal properties

Introduction

In calorimetry, we measure energy or heat power by observing how these values change from an initial stable state. Once the process we want to study begins, the initial state is considered as reference [1]. If the instrument used is differential, the initial baseline is nearly zero. However, if it is not differential, the baseline is not zero [2]. In both cases, it is necessary to correct the calorimetric signal by subtracting the baseline, which is constructed from the initial and final steady states of the measurement, which may coincide or not. Baseline variations may be caused by several factors and require an accurate study to make the appropriate correction, which may be different in each case [3].

In this paper we present a calibration process without baseline correction. Before going into the problem, we illustrate a common process in which baseline correction is necessary (titration calorimetry); and the case of a non-differential skin calorimeter used for assessment of thermal magnitudes of the human skin.

One of the fields where careful management of the baseline is crucial is isothermal titration calorimetry [4]. In our laboratory we have a classical Isothermal Titration Calorimeter (TAM 2277 from Thermometric), that we used for an illustrative experiment. In this experiment, the enthalpy of mixing of ethanol + water is determined. The mixing cell and injection system are prepared, and agitation is set to 120 rpm. Once steady state is reached, ten pulses of 0.15 mL ethanol are injected into 1 mL of initial water. A homogenizing coil maintains the temperature of the liquid to be injected at the same temperature as the thermostat. Figure 1a shows the calorimetric signal corresponding to three identical Joule dissipations (J1–J3) performed to verify the consistency of the calorimeter's sensitivity (396 mVW^{-1}). The response to the 10 injections (M1-M10) is also shown. By inspecting the calorimetric signal when is vertically expanded (blue line in Fig. 1b), a baseline correction is necessary to determine the energies developed in each process. For this, a polynomial which passes through all the initial and final points of each Joule or injection pulse is constructed (red line in Fig. 1b). Once the correction is made (Fig. 1c), the signal is integrated, divided by the sensitivity, and the energy of each process is determined. Note that the baseline variation

✉ Pedro Jesús Rodríguez de Rivera
pedro.rguezderivera@ulpgc.es

[1] Department of Physics, Universidad de Las Palmas de Gran Canaria (ULPGC), Las Palmas de Gran Canaria, Spain

[2] Cardiology Service, Hospital Universitario Marqués de Valdecilla, Santander, Spain

Published online: 03 October 2025

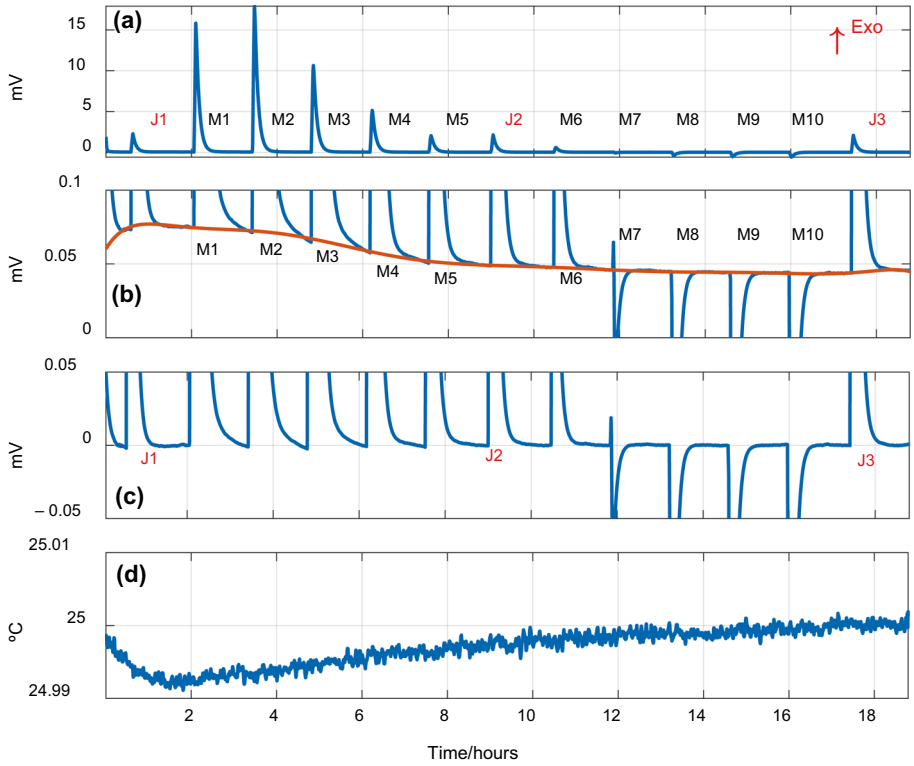

Fig. 1 Illustrative experiment performed in an isothermal titration calorimeter. **a** calorimetric signal corresponding to Joule dissipations (J1–J3) and 0.15 mL ethanol injection pulses over 1 mL water (M1—M10), **b** calorimetric signal zoom (blue line) and baseline adjustment (red line), **c** calorimetric signal zoom with baseline corrected, **d** thermostat temperature during measurement

is consistent with the variation recorded in the thermostat temperature of the calorimeter (Fig. 1d). Table 1 shows the energies calculated for each Joule or injection pulse. With this discussion, we aim to illustrate that a reference is always used when studying an energetic process. In this case, the reference is provided by the baseline.

Despite the great interest of titration calorimetry, in the last years, our group focused on the development of calorimetric sensors, also known as skin calorimeters. This device is a combination of different concepts, including heat conduction calorimeters and differential scanning calorimeters designs. The skin calorimeter is able to determine the heat flux, the heat capacity and the thermal resistance of a 2 × 2 cm^2 skin area, for different temperatures of the calorimeter thermostat. This paper discusses a new calibration method that allows to operate the calorimeter without correcting its baseline. Before getting into the subject, it is necessary to note the two main measurement procedures that have been used until now:

(a) In the first procedure, the measurement begins with the calorimeter on its calibration base. When the calorimeter reaches a steady state at a constant thermostat temperature, it is placed on the skin. Then, the calorimeter is returned to the calibration base. Figure 2 shows the calorimetric signal and the thermostat temperature of a measurement performed on the dorsal area of the right hand of a healthy 24-year-old male subject, seated and at rest. The ambient temperature was 23.2 °C. In this procedure, the power transmitted by conduction between the skin and the thermostat is given by the expression $A_0 + \Sigma A_i \cdot \exp(-t\tau_i^{-1})$ [5]. In this case, the zero power reference corresponds with the time when the calorimeter is on its calibration base. For this case,

Table 1 Calculated energies from the measurement shown in Fig. 1

System ethanol (1) + water (2); $nt = n_1 + n_2$; $x_1 = n_1\, nt^{-1}$; Enthalpy of mixture: $H^E = \sum Ai\ nt^{-1}$													
Measurement	J1	M1	M2	M3	M4	M5	J2	M6	M7	M8	M9	M10	J3
x_1(ethanol)		0.044	0.085	0.122	0.156	0.188		0.217	0.244	0.270	0.294	0.317	
nt /mol		0.058	0.061	0.063	0.066	0.068		0.071	0.074	0.076	0.078	0.081	
Ai/J	**1.989**	14.82	17.98	10.90	5.229	2.096	**2.002**	0.597	− 0.076	− 0.411	− 0.572	− 0.633	**2.000**
∑Ai /J		14.82	32.79	43.69	48.92	51.02		51.61	51.54	51.13	50.55	49.92	
H^E $Jmol^{-1}$		254.9	540.2	690.5	743.0	745.7		727.0	700.6	671.5	642.3	614.2	

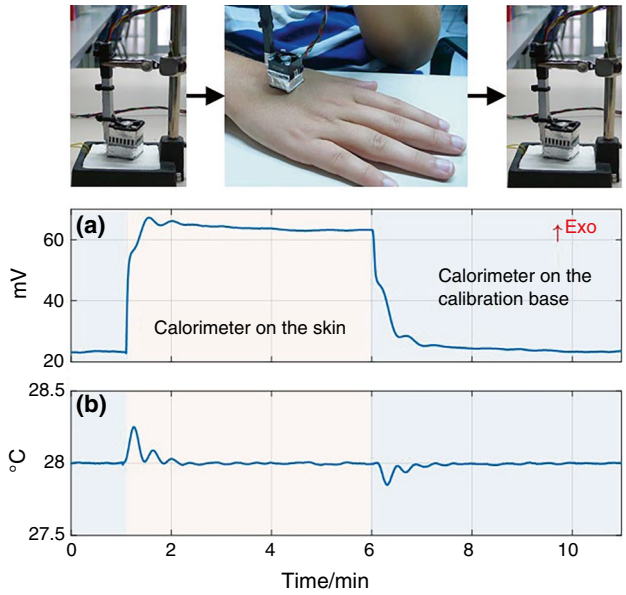

Fig. 2 Skin calorimeter on the calibration base and on the skin. **a**) Calorimetric signal and **b**) thermostat temperature. Measurement procedure in which the calorimeter is on its base ($t < 1$ min), then applied to the skin ($t = 1 - 6$ min) and finally returned to its base ($t > 6$ min)

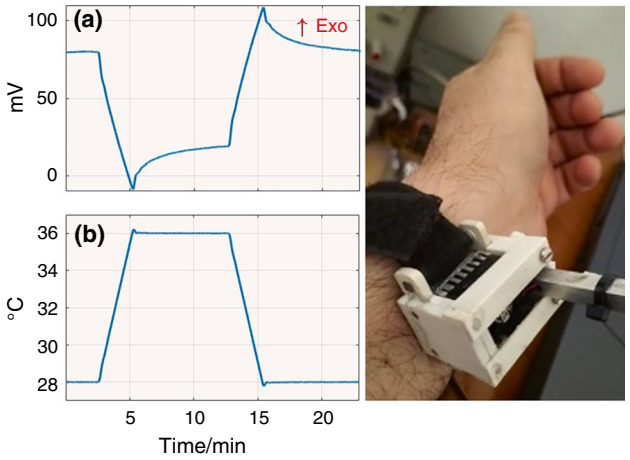

Fig. 3 Calorimeter on the skin with an adapted attachment. **a**) calorimetric signal, **b** thermostat temperature. Measurement procedure in which the calorimeter is applied to the skin at all time

at a thermostat temperature of 28 °C and when the calorimeter was on the skin: $A_0 = 156.6$ mW, $A_1 = 779.3$ mW, $A_2 = 25.4$ mW, $\tau_1 = 3.1$ s, $\tau_2 = 20.0$ s. According to Hansen's classification [6], this operating mode is characteristic of isothermal non-differential heat conduction calorimeters.

(b) The second procedure involves permanently placing the calorimeter on the skin, using a holding system (see Fig. 3). When steady state is reached at the initial thermostat temperature, a linear thermostat temperature change is programmed. When the new temperature steady state is reached, the temperature is returned to the previous value in the same way. Figure 3 shows the calorimetric signal and the thermostat temperature. This type of measurement allows the determination of the skin heat capacity, thermal resistance and heat flux change when the thermostat temperature changes [7]. Figure 3 shows a measurement performed on the volar area of the left wrist of a healthy 64-year-old male subject. The values obtained in this case were $C_{skin} = 2.3$ kJ^{-1}, $R_{skin} = 32.4$ KW^{-1}, and $\Delta W_{skin} = -194.2$ mW. According to Hansen's classification [6], this method corresponds to a non-differential heat conduction calorimeter with a programmable thermostat, similar in operation to the DSC but in this case non-differential.

In clinical practice, it is necessary that the calorimeter is securely attached to the skin area to be measured, but this measurement procedure only allows the determination of the variation of the heat flux relative to the initial state. This is because the calibration is done from a steady state in which the baselines of all input–output variables of the calorimeter have been corrected. These variables are four: the skin and thermostat powers, the calorimetric signal and the thermostat temperature. To determine the calorific powers at each instant—without correcting the baselines—it is necessary to perform a system identification that takes into account all the variables that affect the operation of the calorimeter, including those that are constant during the measurement and are therefore not considered in classical calibrations [8, 9].

After this introduction, in which we discuss the interest of measuring without baseline correction, we give a brief description of the experimental system and the operating model. Then, we present the calibration of the instrument, showing the difference between the parameters that depend only on the instrument and are invariant, and those that depend on the skin of each subject. This paper concludes with the analysis of two interesting experimental measurements at rest and during physical activity. Although this calibration process without baseline correction is complex, it may be useful for devices and applications where a fully differential setup is not possible, especially for wearable thermal sensors.

Experimental system and operating model

The skin calorimeter consists of a measurement thermopile placed between an aluminum measuring plate and a programmable thermostat that consists of an aluminum block, which contains a heating element and a temperature

sensor. The other side of the thermostat is connected to a Peltier element which provides the cold source necessary for temperature control. The Peltier element has an aluminum heatsink and a fan. The thermopile and the thermostat are laterally insulated with expanded polystyrene and shielded from radiation with a layer of reflective aluminum foil. Figure 4 shows an exploded view of the skin calorimeter, and its parts are indicated.

This calorimeter is designed to operate over a wide range of ambient (20–30 °C) and thermostat temperatures (20–40 °C). The input variables of the system are the skin power (W_1), the thermostat power (W_2), the intensity of the Peltier element (I_{pel}) and the ambient temperature (T_{room}). These two variables are not usually considered in calibration because they remain constant during the measurements. In this work, we incorporate these variables in the equations that define the behavior of the calorimeter. We consider a two-body RC model [10]. The first body represents the skin region affected by the measurement, and the measuring plate. The second body represents the thermostat. Each body is characterized by its temperature and heat capacity (T_i and C_i). The bodies are connected with the surroundings and together by thermal conductances P_i and P_{ik}. The calorimetric model (Fig. 4b) is the result of applying the heat conduction equations to each body (1):

$$\begin{aligned} W_1 &= C_1 \frac{dT_1}{dt} + P_{12}(T_1 - T_2) + P_1(T_1 - T'_{room}) \\ W_2 &= C_2 \frac{dT_2}{dt} + P_{12}(T_2 - T_1) + P_2(T_2 - T_{cold}) \end{aligned} \tag{1}$$

The outputs of the system are the thermostat temperature (T_2) and the calorimetric signal (y) provided by the measuring thermopile, which is related (2) with the temperatures of the two sides of the thermopile, trough on the Seebeck coefficient (k):

$$y = k(T_1 - T_2) \tag{2}$$

The temperature on the cold side of the Peltier element (T_{cold}) is proportional to its supply current (I_{pel}). On the other hand, the other side of this Peltier element is cooled by the aluminum heatsink and its fan. This produce a slight temperature rise around the sensor. These phenomena translate into two Eq. (3):

$$\begin{aligned} T_{cold} &= T_{room} + \alpha I_{pel} \\ T'_{room} &= T_{room} + \beta I_{pel} \end{aligned} \tag{3}$$

Combining the above equations we have the following system (4):

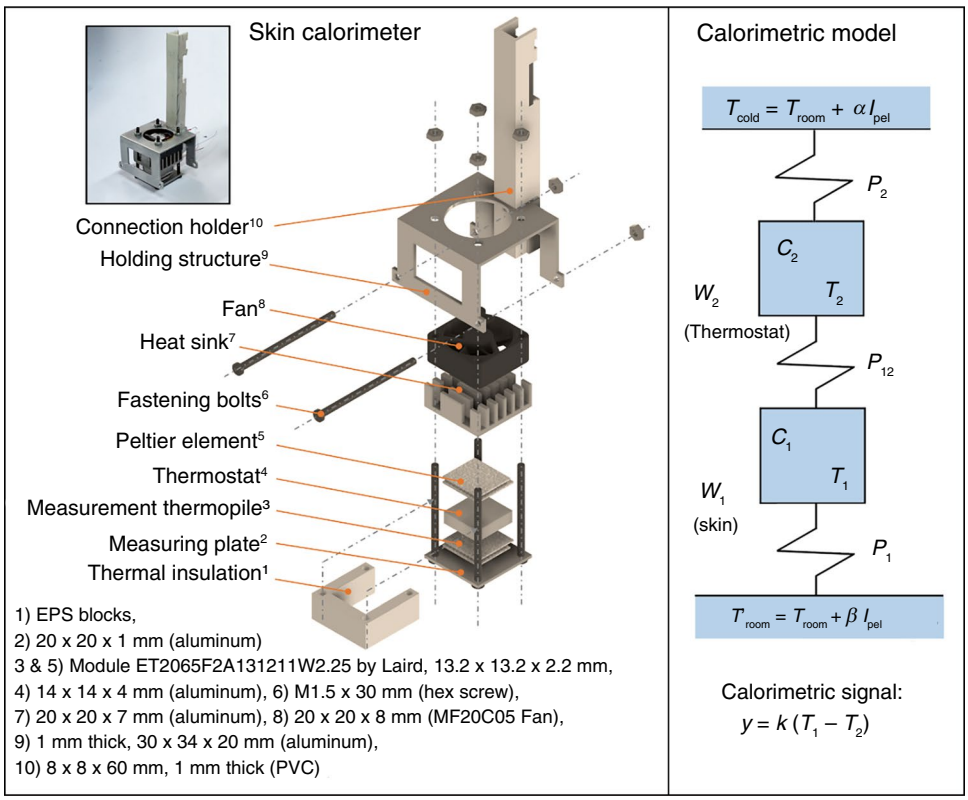

Fig. 4 Skin calorimeter exploded view and calorimetric model scheme. **(1)** EPS lateral insulation, **(2)** Measurement plate, **(3)** Measurement thermopile, **(4)** thermostat, **(5)** Peltier element, **(6)** fastening bolts, **(7)** heat sink, **(8)** fan, **(9)** holding structure, **(10)** connection holder

$$W_1 + P_1 T_{\text{room}} + P_1 \beta I_{\text{pel}} = \frac{C_1}{k}\frac{\mathrm{d}y}{\mathrm{d}t} + \frac{P_1 + P_{12}}{k} y + C_1 \frac{\mathrm{d}T_2}{\mathrm{d}t} + P_1 T_2$$
$$W_2 + P_2 T_{\text{room}} + P_2 \alpha I_{\text{pel}} = -\frac{P_{12}}{k} y + C_2 \frac{\mathrm{d}T_2}{\mathrm{d}t} + P_2 T_2 \quad (4)$$

These equations form the operating principle of the calorimeter, where all the variables can be measured. The parameters to be identified in the calibration are: C_1, C_2, P_1, P_2, P_{12}, k, α and β. The calorimeter's own parameters are invariant. However, the parameters C_1 and P_1 depend on the skin, or the calibration base where the calibration is performed.

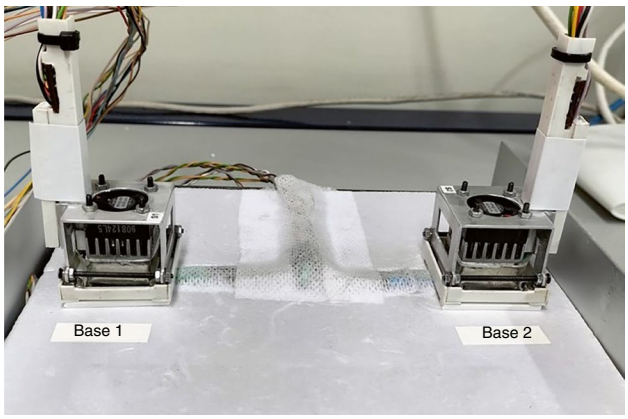

Fig. 5 Skin calorimeters on their calibration base

As noted above, in 2016 we built two skin calorimeters, widely used in several experiments [5, 11] on different subjects. Two new skin calorimeters were produced in 2023 (Fig. 4). These new devices upgrade the previous models in some aspects: higher sensitivity thermopiles (ET20-65-F2A-1312–11-W2.25 from Laird Thermal Systems), a more efficient aluminum heatsink, and a lighter skin attachment system. In this new version, the thermostat can operate from 10 °C below the ambient temperature.

Complete calibration

Calibration is performed with the help of a small aluminum block (10 × 10 × 4 mm) that contains a calibration resistor and a temperature sensor. This block is placed (see Fig. 5) on a calibration base made of insulating material (EPS). In this section we present the calibration of the new calorimeters, called S1 and S2.

For calibration, we performed measurements with control of the calorimetric signal (y), the thermostat temperature (T_2), and with different supplies of the Peltier element (I_{pel}). The goal is to accurately represent the behavior of the calorimeter in various situations, covering its entire operating range. Figure 6 shows a calibration measurement in which we have programmed thermostat temperature pulses (from 26 to 32 ºC) and Joule dissipation pulses in the calibration base (400 mW). These measurements were performed for a

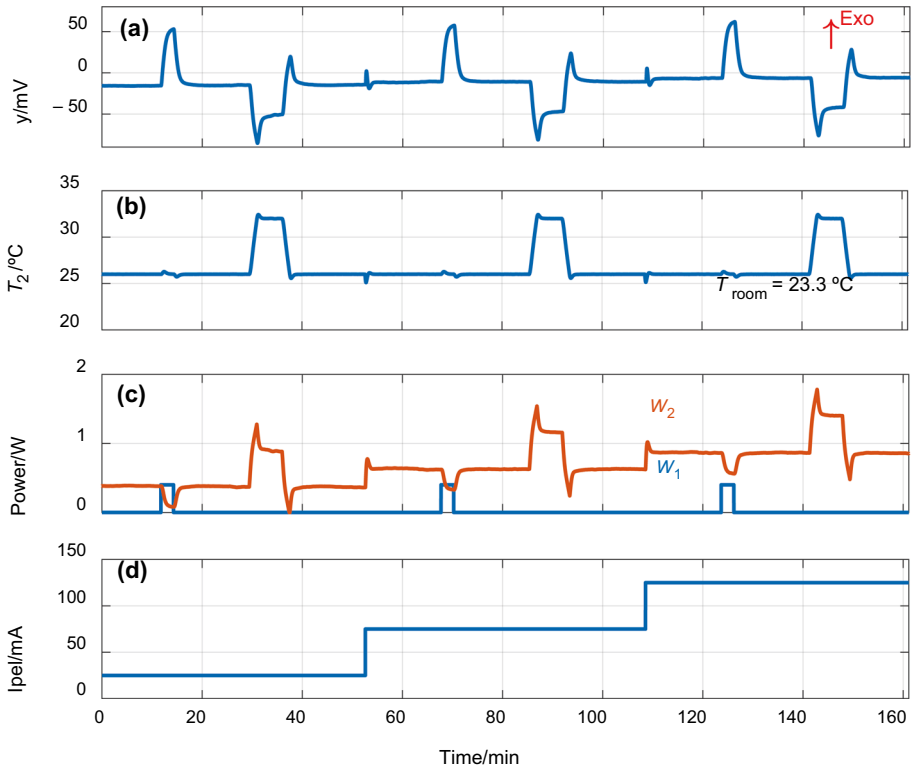

Fig. 6 Calibration measurement with programming of the thermostat temperature (T_2) and power pulses at the calibration base (W_1) for different Peltier currents (I_{pel}). **a** Calorimetric signal (y), **b** thermostat temperature (T_2), *c*) Joule dissipation (W_1) and thermostat power (W_2), *d*) Peltier element intensity (I_{pel})

Peltier supply of 25, 75 and 125 mA. The calorimetric signal and the thermostat power are the result of all programmed excitations. Figure 7 shows a similar measurement, but in this case the calorimetric signal is programmed from 0 to − 50 mV instead of the thermostat temperature. Figure 8 shows a measurement that combines the two previous procedures, but with 40 and 80 mA I_{pel} supply. These three figures represent measurements performed for one of the calorimeters (S1). For the other calorimeter (S2) the measurements are similar.

For the identification of the model parameters, the Nelder-Mead Simplex Method was used with the *fminsearch* function in MATLAB [12, 13]. Using the power curves (W_1 and W_2), the ambient temperature (T_{room}), and Peltier current (I_{pel}); the method calculates the calorimetric signal (y) and thermostat temperature (T_2) by iteratively adjusting the model parameters to minimize the following error criterion:

$$\varepsilon = \varepsilon_y + \varepsilon_{T_2} = \frac{\omega_1}{N}\sqrt{\sum_{i=1}^{N}\left(y_{exp}[i] - y_{cal}[i]\right)^2} + \frac{\omega_2}{N}\sqrt{\sum_{i=1}^{N}\left(T_{2\,exp}[i] - T_{2cal}[i]\right)^2} \quad (5)$$

where experimental values are labeled with the subscript exp, and model-calculated values (Eq. 4) are labeled with the subscript cal. N represents the number of points used in the fitting process, which includes all data from the experimental curves shown in Figs. 6, 7, and 8 (sampling period $\Delta t = 0.5$ s), and ω_1, ω_2 are ponderation parameters (ω_1 in mV^{-1} and ω_2 in K^{-1}). Table 2 shows the calibration results at the calibration base. From the average value of the model parameters, and the curves of the calorimetric signal, thermostat temperature, and Peltier current; we reconstructed the powers W_1 and W_2, obtaining a root mean square error of less than 0.15 mW. This result is considered acceptable.

Applications on the skin

Performing a measurement in the calibration base is different from measuring on the skin. In this last section, we show two applications of the skin calorimeter on the skin. In the first application, the objective is to determine the heat flux in a subject that is seated and at rest. In the second one, the objective is to measure the heat flux in the same subject, while performing moderate exercise on a stair stepper (Fig. 9).

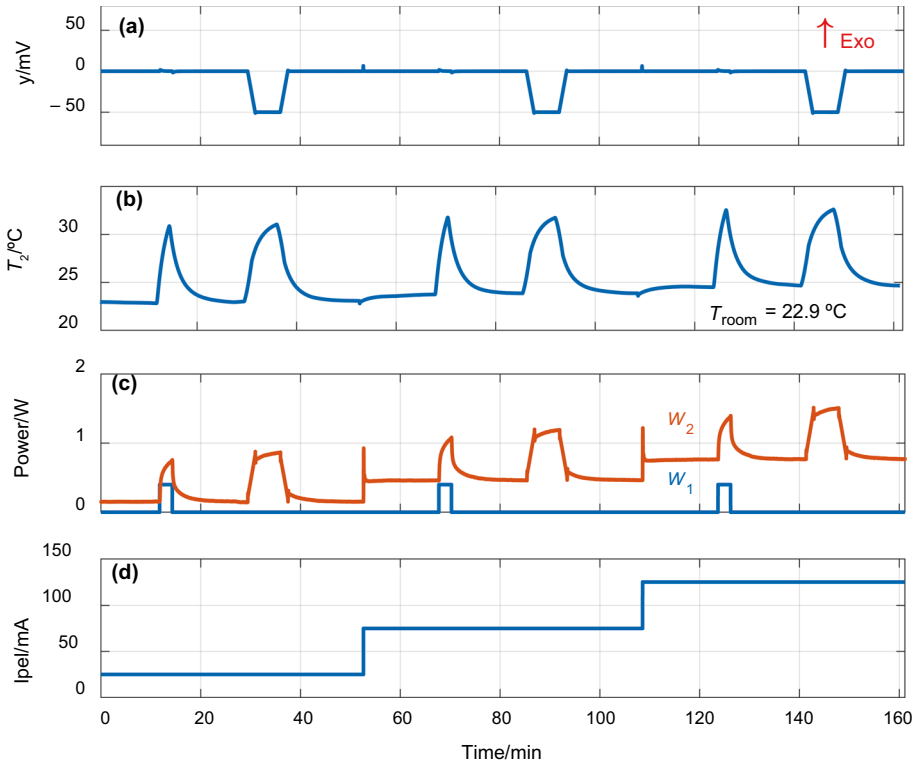

Fig. 7 Calibration measurement with programming of the calorimetric signal (y) and power pulses at the calibration base (W_1) for different Peltier currents (I_{pel}). Thermostat temperature and power (T_2 and W_2). **a** Calorimetric signal (y), **b** thermostat temperature (T_2), **c** Joule dissipation (W_1) and thermostat power (W_2), *d*) Peltier element intensity (I_{pel})

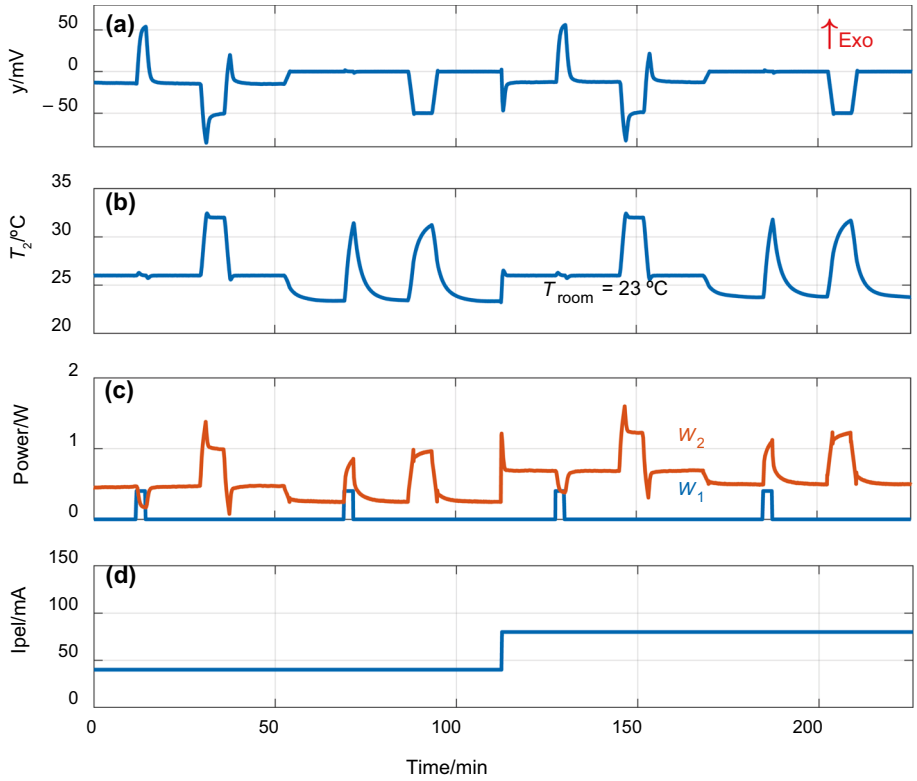

Fig. 8 Calibration measurement with programming of the thermostat temperature (T_2) and the calorimetric signal (y), and power pulses at the base (W_1) for different Peltier currents (I_{pel}). Thermostat power (W_2). **a** Calorimetric signal (y), **b** thermostat temperature (T_2), **c** Joule dissipation (W_1) and thermostat power (W_2), **d** Peltier element intensity (I_{pel})

Table 2 Calibration results for calorimeters S1 and S2. Measurements of the type shown in Fig. 6 (1), Fig. 7 (2) and Fig. 8 (3 and 4)

	C_1/JK^{-1}	C_2/JK^{-1}	P_1/ WK^{-1}	P_2/ WK^{-1}	P_{12}/ WK^{-1}	k/ mV K^{-1}	α/KA^{-1}	β/KA^{-1}	ε_y/ µV	εT_2/ mK
S1										
(1)	4.541	3.449	0.03649	0.06666	0.07471	18.75	– 80.87	11.88	7.4	1.03
(2)	4.496	3.453	0.03498	0.06709	0.06609	17.26	– 79.81	11.60	7.0	0.96
(3)	4.481	3.467	0.03561	0.06652	0.07185	18.27	– 80.99	12.26	5.6	0.77
(4)	4.466	3.455	0.03557	0.06649	0.07158	18.23	– 81.49	11.71	5.5	0.79
Mean	4.496	3.456	0.03566	0.06669	0.07111	18.13	– 80.79	11.86		
Std	0.032	0.008	0.00062	0.00028	0.00360	0.62	0.71	0.29		
S2										
(1)	4.128	3.092	0.03225	0.0565	0.06505	18.16	– 84.70	18.40	7.7	0.99
(2)	3.979	3.034	0.03106	0.05621	0.05664	16.53	– 85.53	17.56	7.2	1.07
(3)	3.996	3.020	0.03219	0.05669	0.06138	17.51	– 83.37	19.51	5.5	0.81
(4)	3.992	3.036	0.03199	0.05623	0.06198	17.61	– 84.59	19.05	5.5	0.80
Mean	4.024	3.046	0.03187	0.05641	0.06126	17.45	– 84.55	18.63		
Std	0.070	0.032	0.00055	0.00023	0.00035	0.68	0.89	0.85		

Root mean square error of the fit for calorimetric signal and thermostat temperature (εy and εT_2 in Eq. 5)

Measurement at rest

In this case, the measured quantities will be the heat flux, the heat capacity and the thermal resistance of the skin area where the measurement is performed. The interest of these measurements is diverse, for example to monitor the temporal evolution of a skin lesion [14], and also to characterize these magnitudes in different areas of the skin, which could be useful in physiology and medicine [15].

In previous works, we developed a methodology to determine these three magnitudes. In the first procedures (Fig. 2), the calorimeter needed several minutes at the calibration base to have a good baseline. This procedure makes it possible to determine the thermal quantities [11], but lacks

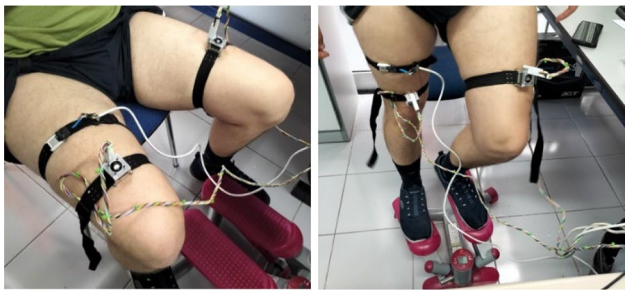

Fig. 9 Placement of the skin calorimeters on a subject at rest and doing moderate physical activity

practical utility. The following procedures don't require this time in the calibration base (Fig. 3), but at the cost of losing information on one of the measurements, the heat flux. In the procedure proposed in this work, the new complete calibration allows to determine the heat flux at every instant without losing information. In all cases, the signal transient responses allow the determination of the heat capacity of the skin; and from the steady states for two different thermostat temperatures, it is possible to determine the thermal resistance of the skin [7].

Now, we show a measurement designed to determine the heat capacity, the thermal resistance and the heat flux of the skin. Two calorimeters were placed on the right (S1) and left (S2) thigh of a healthy 29-year-old male subject (Fig. 9). In this measurement, the thermostat temperature T_2 is periodically programmed between 26 and 36 °C. Figure 10 shows the calorimetric signal and the thermostat temperature T_2.

The model was identified in the previous section (Table 2) but the parameters C_1 and P_1 depend on the subject's skin, and their values must be determined for each skin area and subject. The measurement shown has five pulses, but with one half of a pulse (one of the cooling or heating cycle indicated as 1–10 in Fig. 10) is enough to determine an approximate value of these magnitudes. The heat capacity of the skin is given by the expression: $C_{skin} = C_1 - C_0$, where C_0 is the offset value. This value has been previously calculated, in a measurement with the calorimeter applied on air, which is equivalent to a sample with nearly-zero heat capacity: $C_{0(S1)} = 2.5\ \mathrm{JK}^{-1}$, $C_{0(S2)} = 2.2\ \mathrm{JK}^{-1}$. The thermal resistance of the skin is calculated by the expression $R_{skin} = P_1^{-1}$. To determine the heat flux for a subject at rest, a hypothesis is considered in which the heat flux is given by the following expression (6):

$$W_{skin}(t) = W_{skin}(0) - \frac{\left[T_2(t) - T_2(0)\right]}{P_{12}^{-1} + P_1^{-1}} \tag{6}$$

The values to be determined are C_1, P_1 and the initial value of W_{skin}. However, the identification of the calorimeters was performed at the calibration base. When the calorimeters are placed on the skin, the temperature around the calorimeter increases because of the proximity of the human body, and an increase of this temperature (ΔT_{room}) has to be determined too.

The determination of these four parameters (C_1, P_1 W_{skin} (0) and ΔT_{room}) is performed with the same method used in the calibration: the Nelder-Mead Simplex Method [12, 13]. The slight temporal variability of the skin thermal properties [11] complicates the global adjustment of the transient sections of the experimental curves. For this reason, we identify these parameters in each heating and cooling cycle.

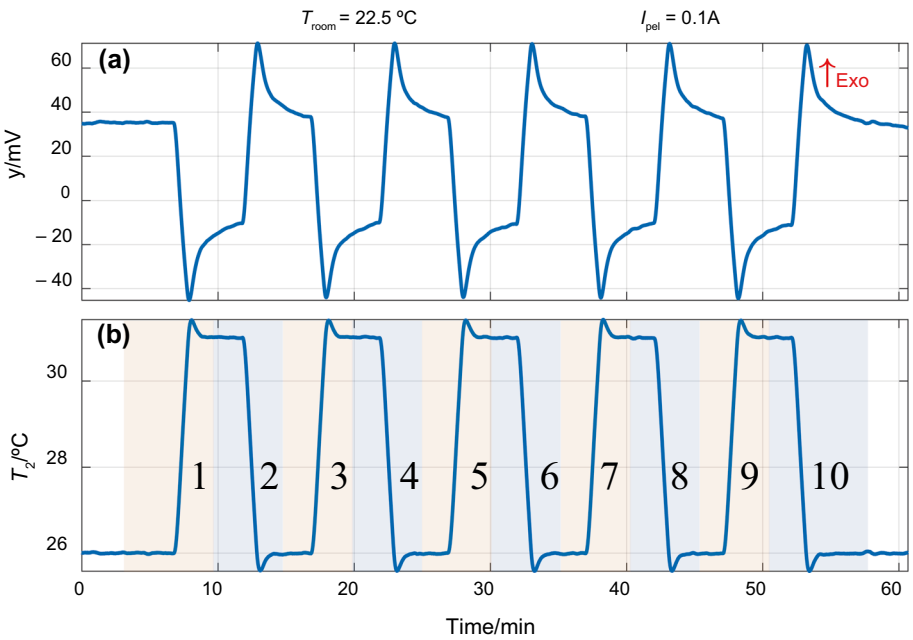

Fig. 10 Measurement performed on the thigh of a healthy 29-year-old male subject at rest. **a** Calorimetric signal and **b** thermostat temperature T_2. Ambient temperature was $T_{room} = 22.5$ °C and Peltier current, $I_{pel} = 0.1$ A. Heating (red)/cooling (blue) cycles indicated as 1–10 (measurement performed with calorimeter S1)

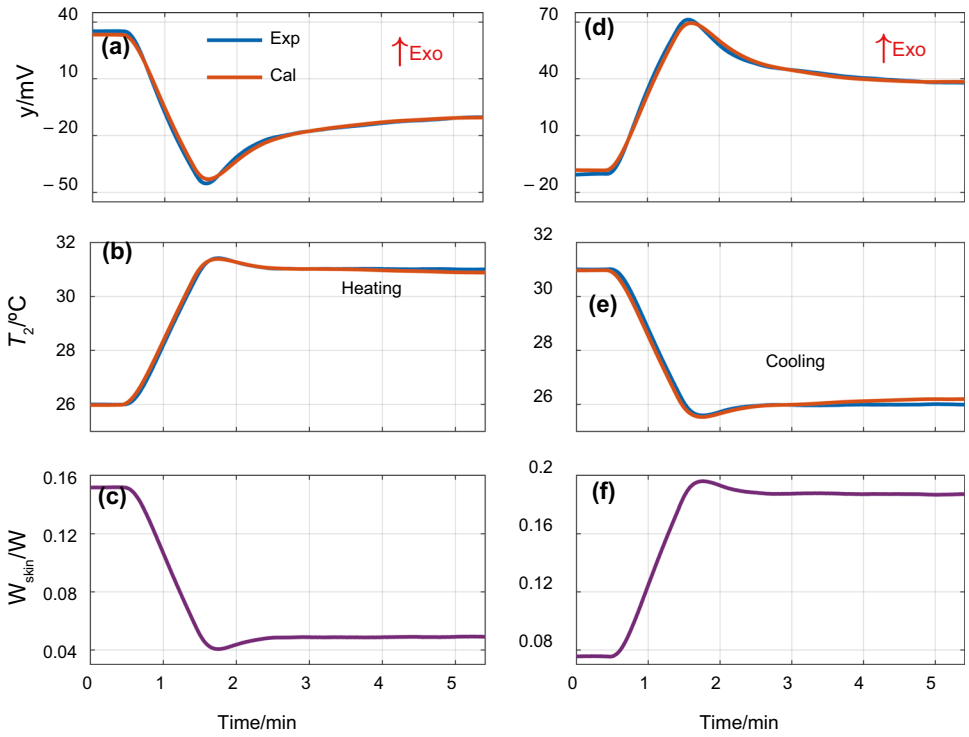

Fig. 11 Iterative process to determine the parameters C_1, P_1, W_{skin} y ΔT_{room} for heating (**a, b, c**) and cooling (**d**, *e*, *f*) of the skin (cycle 1 and 2 in Fig. 10). **a** and **d** calorimetric signal, *y*; **b** and **e**) thermostat temperature T_2 and **c** and **f**) skin heat flux W_{skin} (measurement performed with calorimeter S1)

Figure 11 shows the fittings of the calorimetric signal *y* and the thermostat temperature T_2 for the heating and cooling cases that correspond to the first cycle of the experimental measurement (1 and 2 in Fig. 10b). Figure 11 also shows the heat flux W_{skin} calculated from Eq. 6. Note that the heat flux varies proportionally as a function of the thermostat temperature T_2, as expected. Table 3 shows the results of the identification of the parameters C_1, P_1, W_{skin} and ΔT_{room} for each heating/cooling cycle (1–10 in Fig. 10), and for each calorimeter. For the W_{skin} results, the initial and final heat flux values (W_{1a} and W_{1b}) are shown. The RMSE of the calorimetric signal *y* and the thermostat temperature T_2 (εy and εT_2 in Eq. 5) fittings are also shown, for N = 650 points. As we can see, the parameters C_1 and P_1 are not constant and varies over time, but the deviations from the mean value are low (< 5%).

The hypothesis given by Eq. 6 provides an approximation of the heat flux, but only when the subject is at rest and there are changes in the thermostat temperature T_2. However, if the subject is moving and there is no change in the thermostat temperature, a new calculation procedure is necessary. Now, we describe this new procedure. First, we consider the mean values of the parameters C_1 and P_1, determined in the specific measurements as previously shown. Then, we determine the ambient temperature increase (ΔT_{room}) using the second system equation in Eq. 4. Once the time function of ΔT_{room} is determined, it is substituted into the first system equation in Eq. 4 to determine the heat flux ($W_1 = W_{skin}$). To test the validity of the method, we show the experimental (exp) and model-calculated (cal) thermostat power W_2 with the equation corrected by ΔT_{room} (Fig. 12a). The ΔT_{room} time function is shown in Fig. 12b, and c shows the heat flux determined using the these procedure (Eq. 4, filtering) compared to the hypothesis of Eq. 6 (modelling). From these results, we conclude that for the case of subjects at rest the hypothesis considered (Eq. 6) is acceptable. The derivatives amplify the high frequency noise and a smoothing is necessary and applied in the result shown in Fig. 12c.

Measurement during exercise

In this section we present two experiments, in which we continuously measure in a subject that is performing moderate exercise on a stair stepper. The subject is a healthy 29-year-old male, the same individual from the previous section. The calorimeters are attached to the skin with an adapted holder (Fig. 9). To determine the heat flux, we use the system of equations that describe the calorimeter's operation (Eq. 4) and employ the procedure described at the end of previous section. The main experimental issue is that C_1 and P_1 depend on the subject and the skin area being measured. This issue can be resolved in two ways: (1) consider universal mean values for these parameters, (2) measure these parameters before and after each exercise session to evaluate them and use the average value in the measurement during exercise. In this study, we use the second option.

In the first measurement, the calorimeters are placed on the right thigh and the central forehead area. The exercise

Table 3 Results obtained for each cooling/heating pulse of Fig. 10

	C_1/JK^{-1}	C_{skin}/JK^{-1}	P_1/WK^{-1}	$R_{skin>}$/KW^{-1}	W_{1a}/W	W_{1b}/W	ΔT_{room}/ºC	εy/μV	εT_2/mK
S1									
(1)	6.166	3.666	0.0288	34.76	0.1517	0.0491	3.813	52.4	3.24
(2)	6.281	3.781	0.0324	30.91	0.0755	0.1870	3.801	57.4	5.78
(3)	5.949	3.449	0.0326	30.67	0.1682	0.0566	3.676	54.8	4.29
(4)	6.532	4.032	0.0313	31.92	0.0703	0.1794	3.754	60.2	5.37
(5)	6.539	4.039	0.0305	32.78	0.1646	0.0573	3.600	54.4	2.93
(6)	6.253	3.753	0.0309	32.32	0.0698	0.1777	3.546	55.4	3.43
(7)	6.406	3.906	0.0301	33.18	0.1653	0.0593	3.380	52.5	2.49
(8)	6.242	3.742	0.0299	33.47	0.0714	0.1768	3.248	57.0	2.76
(9)	6.225	3.725	0.0316	31.69	0.1653	0.0556	3.165	56.3	3.63
(10)	6.236	3.736	0.0310	32.26	0.0692	0.1774	3.117	57.2	4.94
Mean	6.283	3.783	0.0309	32.40			3.510		
Std	0.175	0.175	0.0012	1.22			0.265		
S2									
(1)	5.411	3.211	0.0263	37.97	0.1409	0.0490	2.804	47.5	8.00
(2)	5.722	3.522	0.0291	34.40	0.0656	0.1649	3.265	49.5	7.40
(3)	5.509	3.309	0.0288	34.73	0.1595	0.0618	2.728	47.8	9.12
(4)	5.450	3.250	0.0285	35.15	0.0655	0.1629	3.282	54.2	8.34
(5)	5.081	2.881	0.0289	34.66	0.1588	0.0605	2.628	54.4	10.88
(6)	5.291	3.091	0.0284	35.21	0.0710	0.1680	3.060	49.5	8.81
(7)	5.361	3.161	0.0286	34.98	0.1610	0.0631	2.539	54.0	8.24
(8)	5.967	3.767	0.0289	34.63	0.0719	0.1704	3.014	57.8	6.36
(9)	5.521	3.321	0.0274	36.56	0.1579	0.0633	2.508	56.2	8.43
(10)	5.481	3.281	0.0284	35.16	0.0716	0.1692	2.835	51.2	8.38
Mean	5.479	3.279	0.0283	35.35			2.866		
Std	0.239	0.238	0.0008	1.10			0.280		

Identification of parameters C_1, P_1, W_{skin} (initial and final values W_{1a} and W_{1b}) and ΔT_{room}. RMSE of the calorimetric signal y and thermostat temperature T_2 (εy and εT_2) fittings ($N = 650$ points)

is performed for 10 min. The thermostat temperature in both calorimeters is 26º C, and the Peltier power supply is 0.15 A, and the ambient temperature was 22.4º C. The heat flux results are shown in Fig. 13a, and the subject's heart rate in Fig. 13b.

The heat flux in the forehead and thigh are comparable, since they have been obtained simultaneously and at the same thermostat temperature T_2. Before exercise, the heat flux in the forehead (274 mW) is higher than in the thigh (135 mW), which is expectable [11]. The heat flux evolution during exercise is different in the two areas. When exercise begins, the heat flux in the forehead increases slightly (from 274 to 295 mW) and decreases to a lower value than before exercise when the exercise ends (246 mW), which is probably due to the observed evaporation of sweat. However, in the case of the thigh, the heat flux decreases slightly at the beginning of the exercise (from 135 to 120 mW) and then increases even after the exercise to 190 mW, subsequently decreasing to 165 mW, slightly higher than the initial state. During the exercise, a steady state is not reached, so a longer exercise measurement is scheduled, which will be shown in the second case.

The second measurement consists of placing the two calorimeters on the right and left thighs (Fig. 9) and setting different thermostat temperatures: 26ºC on the right thigh calorimeter and 35ºC on the left thigh calorimeter. To avoid upper or lower saturation of the temperature control, the Peltier power supply is set to 0.15 A in S1 and 0.05 A in S2. In this case, the exercise on the stair stepper lasts 20 min and the ambient temperature was 24.3 ºC. Figure 14a shows the heat flux and Fig. 14b shows the subject's heart rate.

The heat flux evolution in both areas is similar but, as expected, is greater in the case of the lower thermostat temperature T_2. The initial heat flux is 130 mW for $T_2 = 26$ ºC and 20 mW for $T_2 = 35$ºC. When exercise begins, the heat flux decreases slightly: from 130 to 120 mW at $T_2 = 26$ ºC and from 20 to 5 mW at $T_2 = 35$ ºC. Then starts to increase up to 250 mW for $T_2 = 26$ °C and 100 mW for $T_2 = 35$ ºC. Finally, the heat flux decreases to a value slightly higher

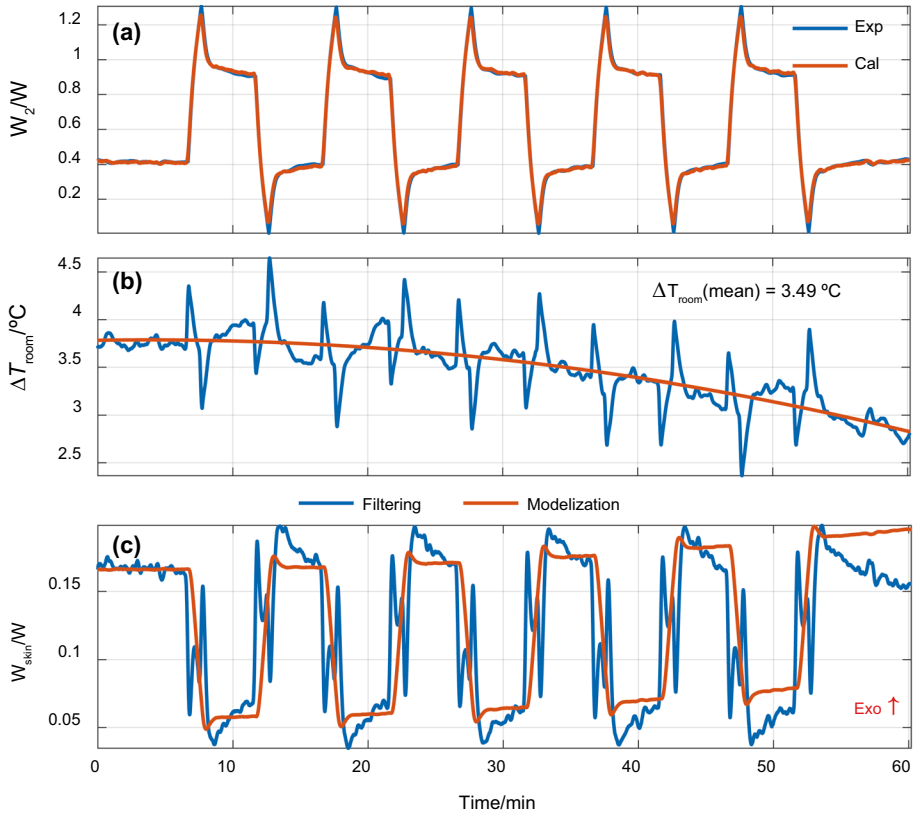

Fig. 12 Skin heat flux determined from the measurement of Fig. 10. **a** experimental exp and model-calculated cal thermostat power W_2, **b** ΔT_{room} calculation, *c*) modelled (Eq. 6) and filtered (Eq. 4) skin heat flux W_{skin} (measurement performed with calorimeter S1)

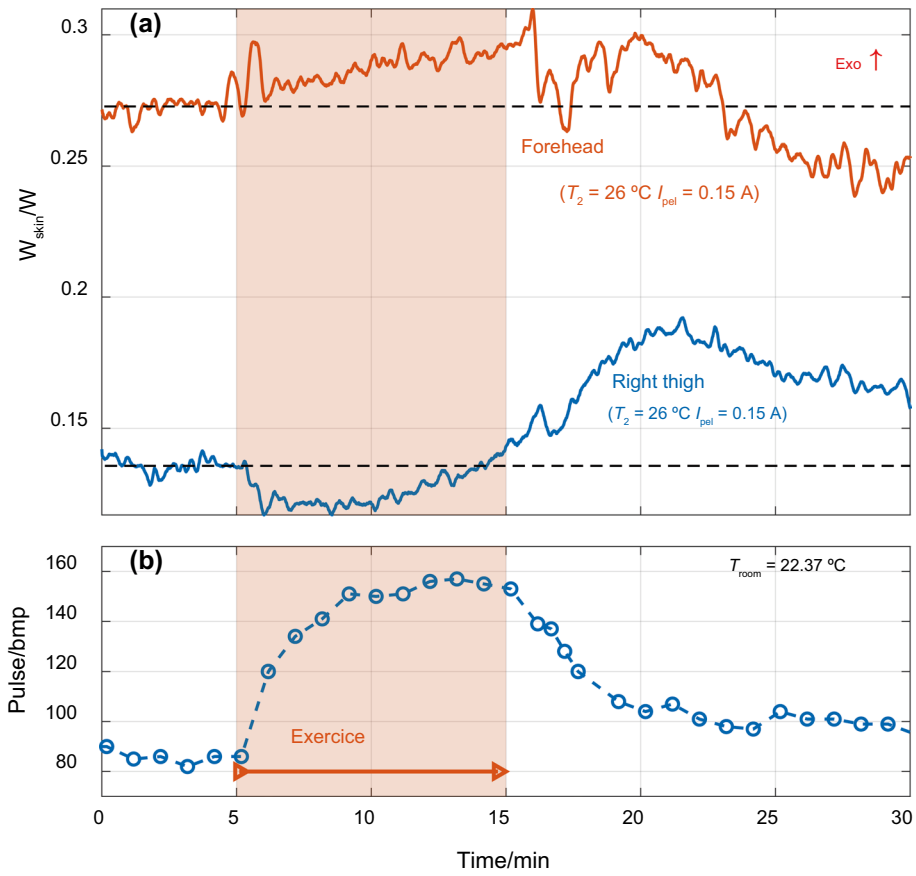

Fig. 13 Heat flux (**a**) and heart rate (**b**) in a simultaneous measurement on the forehead and right thigh of a healthy 29-year-old male subject performing moderate exercise on a stair stepper for 10 min. Mean initial values are indicated by the dash line

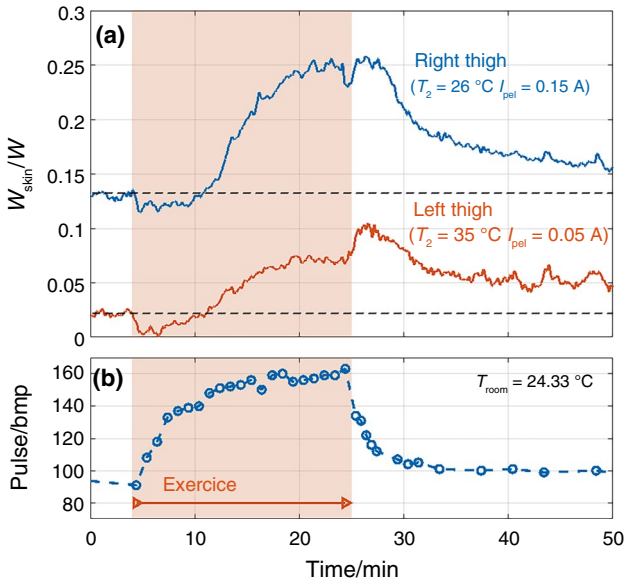

Fig. 14 Heat flux (**a**) and heart rate (**b**) in a simultaneous measurement on the right (T_2 = 26 ºC) and the left (T_2 = 35 ºC) thigh of a healthy 29-year-old male subject performing moderate exercise on a stair stepper for 20 min. Mean initial values are indicated by the dash line

than the initial on: 50 mW for T_2 = 26 ºC and 160 mW for T_2 = 35 ºC.

Next, we briefly discuss the evolution of heat flux when exercise begins. The temporal variation of heat flux during exercise is a dynamic and complex process. We remark the following observations:

- At the beginning of physical exercise, a slight reduction in skin heat flux can be observed in the thigh in all cases studied. This is probably caused by the initial redistribution of blood flow: the body prioritizes blood supply to active muscles to meet their increased oxygen and nutrient demands. This results in a temporary local blood flow reduction in the skin, reducing the skin temperature and consequently the heat flux [11, 16]. The forehead doesn't experience this reduction in heat flux, since it is not an active muscle.
- As exercise continues, the body adjusts its thermoregulatory response to manage the increased heat production. Over time, the body experiences increased heat flux in all parts of the body. This explains the increased heat flux in the forehead [17].
- Regarding the duration of each process, the slight initial reduction of the thigh heat flux lasts about 6 min in the experiments conducted. After that, heat flux increases in all situations, but at different rates. When the exercise ends, the blood flow decreases and everything that was warmed up starts to cool down in a different way. In the forehead, sweating and evaporation cause the heat flux to decrease, and in the thigh, the cooling time constant is higher than in the case of heating, as we can see.

These localized measurements are useful: understanding the temporal variation of heat flux during exercise and the mechanisms that facilitate this heat transfer is essential for optimizing physical performance, and useful in several areas, such as sports medicine [18, 19].

Conclusions

This work introduces a novel calibration method for skin calorimeters, eliminating the need for baseline correction, which is crucial for real-time and continuous monitoring. We conclude that:

1. The calibration process, which involves controlling the thermostat temperature, the power of the calibration element, the Peltier element power supply, and measuring the calorimetric signal; demonstrated high accuracy. The root mean square error in power measurements was less than 0.15 mW. This calibration process enables the device to operate without baseline correction, simplifying the use of skin calorimeters and making them ideal for real-time monitoring of skin conditions and thermal responses during various activities in clinical applications. Experimental measurements were performed on a healthy 29-year-old male subject at rest and during physical activity. The obtained results were consistent with previous studies.
2. During rest, the calorimetric signal and programmed thermostat temperature pulses (26–31 ºC) provided consistent data, allowing accurate determination of skin thermal properties. The mean values and standard deviations for heat flux, heat capacity, and thermal resistance were in line with previous findings, demonstrating the method's reliability for monitoring skin thermal responses in a controlled environment.
3. During exercise, the heat flux measurement exhibited interesting dynamic responses. Initial heat flux values on the forehead and thigh at thermostat temperature of 26 ºC were 274 and 135 mW, respectively (for a surface of 4 cm^2). At thermostat temperature of 35 ºC, the thigh heat flux was initially 20 mW (for a surface of 4 cm^2). A slight reduction in thigh heat flux was observed at the beginning of exercise, likely due to local blood flow redistribution to active muscles. This was followed by a gradual increase in heat flux, particularly in active muscle areas, confirming the device's capability to track real-time changes in skin thermal response during physi-

cal activity. These observations are consistent with the literature.

This calibration method significantly enhances the practical utility of skin calorimeters, offering a reliable tool for continuous and accurate monitoring in various clinical and physiological applications. One limitation of this study is that it includes data from a single subject. The main objective, however, is to determine heat flux before, during, and after the process under controlled conditions, either at rest or during exercise. Further studies with larger samples are needed to assess its clinical relevance. Given the time and complexity involved in extensive human trials, we consider it appropriate to present the research at this stage, as it provides a valuable basis for future simulations and experimental validation.

Funding This research was funded by the Government of the Canary Islands through the "Convocatoria 2024 de Subvenciones para la realización de Proyectos de I+D Aplicada (Modalidad B), en el marco de la Estrategia de Especialización Inteligente de Canarias RIS-3 Ampliada, y cofinanciado por el Fondo Europeo de Desarrollo Regional (FEDER) 2021–2027" Project: "Monitorización de la capacidad calorífica y la resistencia térmica de la piel mediante un calorímetro de piel (SKINCAL)" ID: ProID2024010002.

Declarations

Competing interest The authors declare that they have no known competing financial interests or personal relationships that could have appeared to influence the work reported in this paper.

References

1. Bracken DS, et al. Application Guide to Safeguards Calorimetry. Los Alamos National Laboratory Manual LAUR02–1764. 2002. https://www.researchgate.net/publication/242170728_Application_Guide_to_Safeguards_Calorimetry. Accessed 10 july 2024.
2. Warrington SB, Höhne GWH. Thermal analysis and calorimetry. In: Ullmann's Encyclopedia of Industrial Chemistry. Weinheim: Wiley-VCH Verlag GmbH & Co. KGaA. 2000. https://doi.org/10.1002/14356007.b06_001.pub3.
3. Wu M, Johannesson B, Geiker M. Determination of ice content in hardened concrete by low-temperature calorimetry. J Therm Anal Calorim. 2014. https://doi.org/10.1007/s10973-013-3520-6.
4. Tellinghuisen J, Chodera JD. Systematic errors in isothermal titration calorimetry: concentrations and baselines. Anal Biochem. 2011. https://doi.org/10.1016/j.ab.2011.03.024.
5. Socorro F, Rodríguez de Rivera PJ, Rodríguez de Rivera M, Rodríguez de Rivera M. Mathematical model for localised and surface heat flux of the human body obtained from measurements performed with a calorimetry minisensor. Sensors. 2017. https://doi.org/10.3390/s17122749.
6. Hansen LD. Toward a standard nomenclature for calorimetry. Thermochim Acta. 2001. https://doi.org/10.1016/S0040-6031(01)00422-1.
7. de Rodríguez Rivera PJ, de Rodríguez Rivera M, Socorro F, de Rodríguez Rivera M. Experimental study of the thermal probing depth of a skin calorimeter. Int J Heat Mass Transf. 2023. https://doi.org/10.1016/j.ijheatmasstransfer.2023.124258.
8. Schneidewind J, Olickel H. Improving data analysis in chemistry and biology through versatile baseline correction. Chem Methods. 2021. https://doi.org/10.1002/cmtd.202100005.
9. Darnell A, Leito I, Sikk L, Porosk L. Uncertainty of small enthalpy effects measured by isothermal calorimetric titration. J Chem Metrol. 2021. https://doi.org/10.25135/jcm.57.21.03.1994.
10. Lerchner J, Wolf G, Auguet C, Torra V. A simple tool for the modeling of heat flow calorimeters. Thermochim Acta. 2004. https://doi.org/10.1016/j.tca.2003.06.002.
11. de Rodríguez Rivera PJ, de Rodríguez Rivera M, Socorro F, et al. Heat flow, heat capacity and thermal resistance of localized surfaces of the human body using a new calorimetric sensor. J Therm Anal Calorim. 2022. https://doi.org/10.1007/s10973-021-11062-0.
12. Lagarias JC, Reeds JA, et al. Convergence properties of the nelder-mead simplex method in low dimensions. SIAM J Optim. 1998. https://doi.org/10.1137/S1052623496303470.
13. https://es.mathworks.com/help/matlab/ref/fminsearch.html Accessed, on July 2024.
14. de Rodríguez Rivera PJ, de Rodríguez Rivera M, Socorro F. Monitoring of some minor human skin lesions using a skin calorimeter. J Therm Anal Calorim. 2024. https://doi.org/10.1007/s10973-024-13204-6.
15. Okabe T, Fujimura T, Okajima J, et al. First-in-human clinical study of novel technique to diagnose malignant melanoma via thermal conductivity measurements. Sci Rep. 2019. https://doi.org/10.1038/s41598-019-40444-6.
16. Trangmar SJ, Chiesa ST, Kalsi KK, et al. Whole body hyperthermia but not skin hyperthermia accelerates brain and locomotor limb circulatory strain and impairs exercise capacity in humans. Physiol Rep. 2017. https://doi.org/10.14814/phy2.13108.
17. Sánchez-Delgado G. Brown adipose tissue and exercise: implications on human energy balance and metabolism. The Actibate study. 2018. Universidad de Granada.
18. Bahr R, Bärtsch P, Bourdon L, Calbet JAL, et al. International Olympic Committee consensus statement on thermoregulatory and altitude challenges for high-level athletes. Br J Sports Med. 2012. https://doi.org/10.1136/bjsports-2012-091296.
19. Butts CL, Luhring KE, Smith CR, et al. Effects of mild hypohydration on cooling during cold-water immersion following exertional hyperthermia. Eur J Appl Physiol. 2016. https://doi.org/10.1007/s00421-016-3329-7.